John von Neumann Institute for Computing

Supercomputer Based *ab initio* Investigations of Martensitically Transforming Alloys

Peter Entel, Waheed A. Adeagbo, Alexey T. Zayak,
and Markus E. Gruner

published in

NIC Symposium 2006 ,
G. Münster, D. Wolf, M. Kremer (Editors),
John von Neumann Institute for Computing, Jülich,
NIC Series, Vol. **32**, ISBN 3-00-017351-X, pp. 159-166, 2006.

http://www.fz-juelich.de/nic-series/volume32

Supercomputer Based *ab initio* Investigations of Martensitically Transforming Alloys

Peter Entel[1], **Waheed A. Adeagbo**[1,2], **Alexey T. Zayak**[3], **and Markus E. Gruner**[1]

[1] Theoretische Physik, Universität Duisburg-Essen
Campus 47048 Duisburg, Germany
E-mail: {entel,adeagbo}@thp.uni-duisburg.de

[2] Lehrstuhl für Theoretische Chemie, Ruhr-Universität Bochum
Universitätsstraße 150, 44780 Bochum, Germany
E-mail: waheed.adeagbo@theochem.ruhr-uni-bochum.de

[3] Department of Physics and Astronomy, Rutgers University
Piscataway, NJ 08854-8019, U.S.A.
E-mail: zayak@physics.rutgers.edu

We give a short review of first-principles computational investigations carried out on the high-performance supercomputer facility JUMP at the Forschungszentrum Jülich. Within the framework of Density Functional Theory (DFT) and Density Functional Perturbation Theory (DFPT) we calculate force constants and phonon spectra of various Heusler alloys and Fe based Invar materials using the Vienna *Ab Initio* Simulation Package (VASP) and the Plane Wave Self-Consistent Field (PWSCF) method.

1 Introduction

Recent technological developments concerning "smart materials" show that a microscopic understanding on an *ab initio* basis is needed, for example, for a breakthrough in the field of magnetic shape memory (MSM) alloys recently discovered[1]. Magnetic Heusler alloys exhibit the MSM effect with magnetic-field-induced strains up to 10%, which opens a field of tremendous technological applications. In order to understand this effect, a detailed knowledge of the difference between structurally stable and unstable Heusler alloys on a microscopic scale is needed. In this investigation we concentrate on two kinds of systems, ternary Heusler alloys and binary alloys like Fe_3Ni and Fe_3Pt, which in turn will be shown to behave in similar manner to the Heusler systems.

2 Method

2.1 First-Principles Calculations

The Vienna ab inito Simulation Package[2,3] (VASP) has been used to perform the electronic structure calculations. The projector-augmented wave formalism (PAW) implemented in this package[3] leads to very accurate results comparable to other all-electron methods. The electronic exchange and correlation are treated within density functional theory by using the generalized gradient approximation. The expansion of the electronic wave-functions in terms of plane waves was done using the "High Precision" option, which corresponds to the kinetic energy cutoff as high as 337.3 eV or more, depending on the system. Integrations

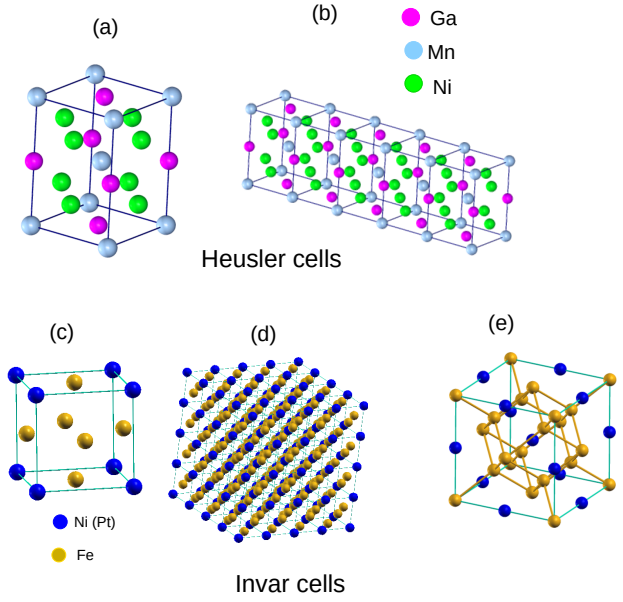

Figure 1. On top: (a) A conventional tetragonal cell used in the electronic structure calculation of Heusler alloys and (b) corresponding supercell used in the phonon calculation. All Hesuler compounds considered in this work have the same structure and formula unit X_2YZ. Below: (c) The $L1_2$(Cu_3Au) structure with unit cell of space group $Pm\bar{3}m$ number 221, (O_h^1 cubic) of Fe_3Ni (Fe_3Pt) used in the electronic structure calculations. (d) The $4 \times 4 \times 4$ supercell containing 256 atoms (192 Fe- and 64 Ni-atoms) used in the direct force constants method for the calculation of phonon dispersions using the packages PHONON[4]+VASP[2] and (e) the $D0_3$ structure (bcc) with unit cell space group $Fm\bar{3}m$ (O_h^5) of $AlFe_3$[5].

over the whole Brillouin zone were performed using special k-points. For Heusler alloys, the electronic structure calculations were done using the conventional tetragonal cell (see Fig. 1(a)) with a high density of k-point mesh of $12\times12\times10$ points. For the phonon calculations in a $1\times5\times1$ supercell (see Fig. 1(b)) the k-points mesh was $10\times2\times8$. While the dimensions of the supercell are given with respect to the conventional tetragonal cell.

For binary alloys of Fe_3Ni and Fe_3Pt (fcc cell of $L1_2$ and bcc-like $D0_3$ structures, see Fig. 1(a and c)) we used a Monkhorst-Pack grid of $12\times12\times12$ k-points while a $2\times2\times2$ mesh was used for the phonon calculations of fcc Fe_3Ni shown in Fig. 1(d).

2.2 Phonon Calculations

2.2.1 Direct Method

In order to calculate the phonon dispersions we have used the direct force constant method[4] with forces determined from total energy calculations by using the Hellmann-Feynman theorem. The reference lattice parameters ($a = b = c$) refer to the conventional cubic (CC) $L2_1$ structure of the Heusler alloys, all crystallographic directions in this work are specified with respect to the CC cell. While the calculations were done using smaller conventional tetragonal (CT) cell with lattice parameters $a_t = b_t = a/\sqrt{2}$, $c_t = c$ (see Fig. 1(a)).

System	a_{L1_2} (Å) (fcc)	a_{D0_3} (Å) (bcc-like)
Fe_3Ni	3.58785644	5.71118938
Fe_3Pt	3.60052116	5.93777408

Table 1. Lattice parameters obtained from VASP calculations for the $L1_2$ (fcc) and the $D0_3$ (bcc-like) structure for Fe_3Ni and Fe_3Pt in the ferromagnetic state.

The phonon calculations for Heusler alloys were done with an elongated $1\times5\times1$ supercell based on the CT cell, see Fig. 1(b). The supercell is subject to periodic boundary conditions and has orthorhombic symmetry. Five CT cells were joined together along [110] giving ten subsequent (110) atomic planes along the [110] direction. Displacements of each single atom induce forces acting on all other atoms within the supercell, which yields the force-constant matrix and, consequently, the phonon frequencies and corresponding eigenvectors. In this work, $1\times5\times1$ geometry yields five points in the Brillouin zone along the [110] direction where phonon parameters are exact. These five vectors satisfy $\exp(2\pi\imath\mathbf{k}_L\cdot\mathbf{L})=1$, where L denotes indices of the lattice constants in the supercell (in our case from 0 to 4, giving points $\zeta=0.0, 0.25, 0.5, 0.75, 1.0$, for the normalized wave vector $[\zeta,\zeta,0]$, which spans our Brillouin zone from its center to the boundary). For the $1\times5\times1$ supercell, within the half supercell length (five atomic planes), the force constants decrease by several orders of magnitude, thus being sufficient for accurate calculations of the phonons. The atomic displacements were of the order of 0.03 Å. The force constants have been calculated for the relaxed and completely force-free equilibrium structures, the lattice parameters of which are given in Table 1.

The method is also applied to fcc Fe_3Ni to calculate phonons along high symmetry directions for the $L1_2$ structure (see Fig. 1(c)) at lattice constant 3.58795644 Å obtained from VASP calculations. The supercell used in the phonon calculation was a $4\times4\times4$ periodic supercell (see Fig. 1 (d)).

2.2.2 Linear Response

In the linear response method the dynamical matrix is obtained from the modification of the electron density, via the inverse of the dielectric matrix describing the response of the valence electron density to a periodic lattice perturbation. The dielectric matrix is then calculated from the eigenfunctions and energy levels of the unperturbed system[14]. Phonon dispersions can be determined at any wave vector in the Brillouin zone. The method has been applied with success to Ni_2MnGa[6] and to alloys related to our present study[6,7].

We have applied this method to calculate the phonon density of states of Ni_2MnGa (reproducing the anomalous inversion of optical modes found previously by using the direct method[8]) and the phonon dispersions along high symmetry for bcc-like $D0_3$ Fe_3Ni, $L1_2$ Fe_3Pt and $D0_3$ Fe_3Pt (crystal structures are shown in Fig. 1(c) (for fcc) and Fig 1(e)). The phonon calculations were carried out again at the theoretical lattice constants shown in Table 1.

For Fe and Ni in Fe_3Ni we used ultrasoft pseudo-potentials generated using the exchange correlation of Perdew-Burke-Ernzerhof (PBE); for Fe and Pt in Fe_3Pt we used pseudo-potentials generated using exchange correlation of Perdew-Zunger (see Ref. 14 for the source).

System	a_{L2_1} (Å)	$\mu_{total}(\mu_B)$	$L2_1$	Magn. order	e/a
Co_2MnGa	5.7100	4.14	stable	FM	7.000
Co_2MnGe	5.7285	4.99	stable	FM	7.250
Ni_2MnGa-e	5.4647	4.20	unstable	FM	7.250
Co_2MnGe+e	6.1957	6.02	-	FM	7.500
Ni_2MnGa	5.8067	4.35	unstable	FM	7.500
Ni_2MnAl	5.7000	4.20	unstable	FM	7.500
Ni_2MnIn	6.0624	4.22	unstable	FM	7.500
Ni_2MnGa+(e/2)	5.8668	3.96	unstable	FM	7.625
Ni_2MnGe	5.8039	4.10	unstable	FM	7.750
Ni_2MnSi	5.6041	3.78	unstable	FM	7.750
Ni_2CoAl	5.6041	1.78	unstable	FM	8.000
Ni_2CoGa	5.6865	1.54	unstable	FM	8.000
Ni_2CoGe	5.7067	1.45	unstable	FM	8.250
Ni_2CoSb	5.9411	1.34	unstable	FM	8.500
Cu_2MnAl	5.9153	3.51	unstable	FM	7.75
Cu_2MnGa	5.9701	3.61	stable	FM	7.75
Cu_2MnSn	6.1674	3.89	unstable	FM	8.00
Ni_2FeGa	5.7554	3.29	unstable	FM	7.75
Ni_2MnSn	6.0576	4.05	unstable	FM	7.75
Co_2FeGa	5.7177	5.02	stable	FM	7.50
Co_2MnSn	5.9837	5.03	stable	FM	7.50
Ni_2TiGa	5.8895	0.00	unstable	NM	6.75
Fe_2MnGa	5.6882	2.15	stable	Ferri	6.50

Table 2. Computed lattice parameters, magnetic moments per unit cell, types of magnetic order and valence-electron-to-atom ratios, e/a, for a series of Heusler compounds with the $L2_1$ structure (Ref. 8). 'Instability' of the cubic structure means here that a soft mode appears in the calculated phonon dispersion.

In both alloys we used a kinetic energy cutoff of 50 Ry for the plane wave basis set. The augmentation charges requiring the use of ultrasoft pseudo-potentials were expanded with energy cutoff of 600 Ry which is high enough to yield accurate results. Structural properties and most of the phonon frequencies are well converged using a first-order smearing parameter $\sigma = 0.02$ Ry for the BZ integration. For self-consistent and non-self-consistent calculations, a Monkhorst-Pack grid of $12\times12\times12$ k-points was used. A set of special $\mathbf{q}$-points in the BZ with finite weight generated from Monkhorst-Pack was used for both the fcc and the simple cubic cell. For the fcc structure we used a $4\times4\times4$ $\mathbf{q}$-point mesh yielding 8 sets of $\mathbf{q}$-vectors with finite weight while for the simple cubic, a $2\times2\times2$ $\mathbf{q}$-point mesh was used yielding 4 sets of special $\mathbf{q}$-vectors.

3 Results and Discussions

3.1 Heusler Alloys

With the help of the supercomputer facilities of the Forschungszentrum Jülich we succeeded to obtain phonon dispersions and the electronic structure of 27 different Heusler

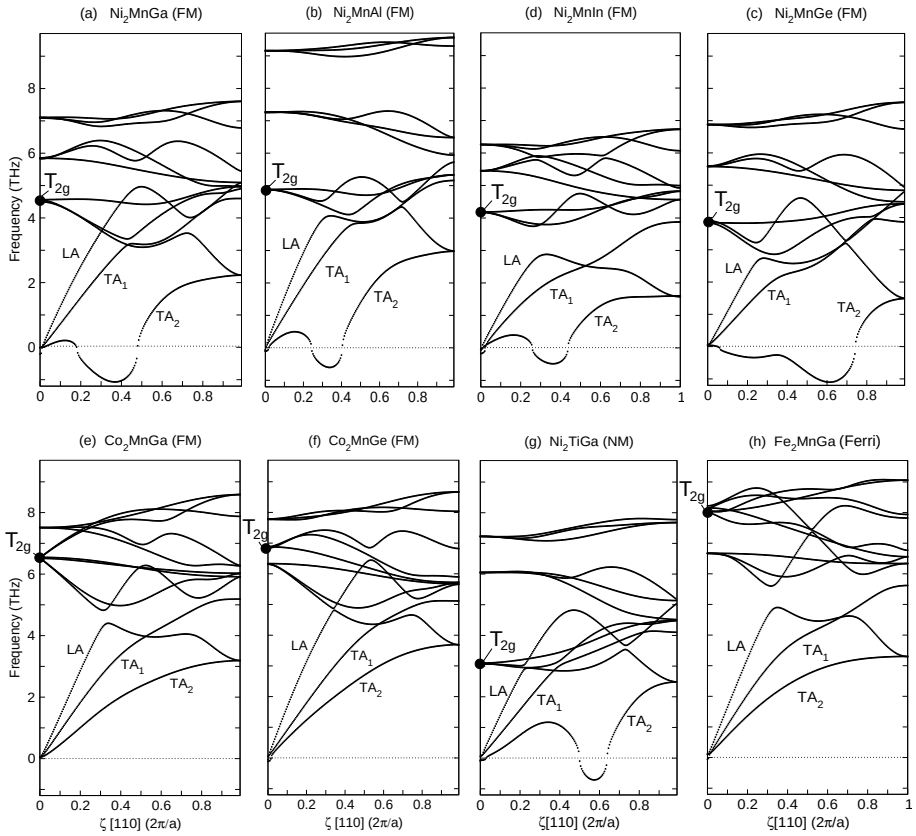

Figure 2. Phonon dispersion curves of (a) FM Ni_2MnGa, (b) FM Ni_2MnAl, (c) FM Ni_2MnGe, (d) FM Ni_2MnIn (e) FM Co_2MnGa, (f) FM Co_2MnGe, (g) NM Ni_2TiGa and (h) FerriM Fe_2MnGa in the $L2_1$ structure. Here, the reduced wave vector coordinate ζ spans the fcc Brillouin zone from Γ to X. Imaginary frequencies of the unstable modes are shown in the real negative frequency range. The frequency of the optical modes T_{2g} at Γ is marked by a black dot; note that it appears at lower values as compared to the stable systems.

structures listed in Table 2. Fig. 2 shows the dispersion curves of 8 of them. Comparison of the phonon dispersions of Ni_2MnGa with existing experimental data and calculations by other groups employing the linear response method show that the direct method used here yields fairly accurate results[6,9].

For the five compounds Ni_2Mn(Ga, Al, In, Ge) and Ni_2TiGa, the TA_2 branch is unstable for some range of ζ. In addition, in Ni_2MnGe the TA_2 mode has a negative slope at Γ, indicating a pure elastic instability. The instability of the $L2_1$ structure in NM Ni_2TiGa shows that magnetic order is not a necessary condition for the phonon softening to occur.

Figure 3 shows the force constants vs. e/a ratio for various Heusler alloys listed in Table 2. Note that negative force Ni-Ni constants in Ni-based compounds are responsible for the structural instability of the compounds. This leads also to inverted optical modes, i.e., Ni vibrates with lower frequency compared to the heavier Ga in the optical frequancy range. Ni vibrations are also Raman active. The Co-based systems have postive force constants and do not undergo a martensitic transformation.

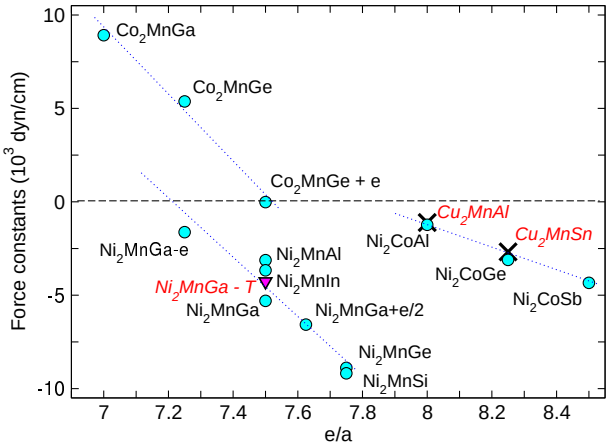

Figure 3. The plot of Ni-Ni and Co-Co force constants vs. e/a ratio for various Heusler alloys. The structurally unstable alloys have negative Ni-Ni force constants.

4 Fe Based Binary Alloys

The second part of this paper is concerned with Fe based binary alloys, in particular the bcc phase of Fe_3Ni.

The most prominent feature in fcc phonon dispersions, which is similar to some of the unstable Heusler alloys, is the instability of the TA acoustic mode which begins at about one third of the length of the wave vector from Γ and extends to the zone boundary M where the softening is highly pronounced. The region Γ-M corresponds to the [110] direction in which the elastic softening has been observed from most experiments[11–13].

It is known from experiment that the bcc phase of Fe_3Ni is the stable phase. The bcc phonon dispersion relations obtained from linear response calculations for Fe_3Ni show different features. As expected, the structure is perfectly stable as none of the phonon branches in the three windows corresponding to [100], [110] and [111] directions show softening unlike in the case of fcc dispersions. In this case the partial contributions of the atoms in the optical range of vibrations obey the expected order, whereby the heavier Ni atoms vibrate at relatively low frequency as compared to Fe.

This behaviour has been a subject of systematic experimental investigations for Fe_3Ni[10]. Inelastic neutron scattering data clearly showed excess states of Ni at relatively lower energies of the optical range in agreement with what we obtained from the calculations.

4.1 Comparison of the Methods

Our comparative study includes analysis of the methods we are using. The two techniques of calculating phonons lead to very similar results, but certain differences appear (not to be discussed here). Taking advantage of working on a supercomputer, we calculated for a large supercell of Ni_2MnGa (216 atoms) in order to obtain accurate vibrational densities of

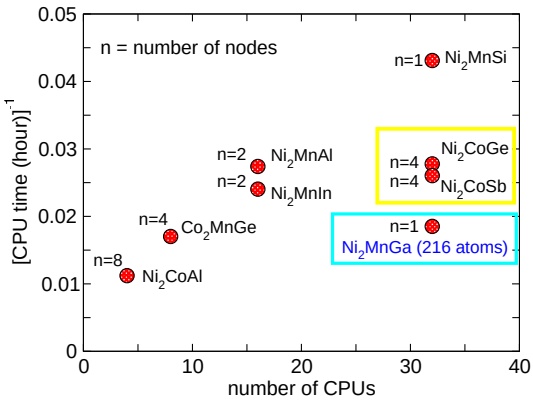

Figure 4. The inverse of CPU time versus the number of tasks per node for the phonon calculation of Heusler alloys with 40 atoms using VASP.

states and compare them with what we get from the linear response calculations. We find that both techniques show good agreement.

4.2 Performance Issues

The calculations presented in this work were carried out on the JUMP (IBM p690) supercomputer at the Forschungszentrum Jülich. From our test calculations we know that 32 processors taken on a single node is the optimal choice for our plane-wave calculations with a 40 atoms cell. However, there are some specific demands on the hardware, which are common to plane-wave codes. Especially for our calculations, we need a large amount of main memory and there is a lot of data transfer between processors. Keeping this in mind, we have done some additional calculations, showing that the data exchange between different nodes of JUMP decreases the efficiency of the calculations considerably. Figure 4 presents data of several test we did by taking our standard 40 atoms supercell with different Heusler systems. We took 32 processors for each of these calculations, but distributed processors among several nodes.

The situation changes, if we want to do calculations with larger cells. Our tests with a 216 atoms supercell have shown that 32 processors are not sufficient to achieve results in reasonable time. On the other hand the distribution over the nodes becomes more efficient. Again, the best choice is if we take complete nodes.

One has to be aware of some difficulties related to input parameters, which VASP code provides in order to control the parallization of the code. A bad choice of the parameters may lead to a significant reduction of the performance. Figure 4 shows such a breakdown, which we experienced in the case of Heusler systems Ni_2CoGe and Ni_2CoSb, when we used 128 processors. Using $NPAR = 128$, which tells vasp to distribute all bands during over the processors, the calculations were even slower than on 32 processors.

5 Concluding Remarks

From this study we have found general properties responsible for structural instabilities in Heusler compounds and Fe-based binary alloys.

Our rough estimate of the supercomputer performance allows to suggest that further investigations in this project may include calculations with very large supercells allowing the treatment of imperfections in the martensitic structure like twin variants.

Acknowledgments

We thank the NIC for providing the supercomputer facilities to perform *ab initio* supercell calculations of magnetic shape memory alloys.

References

1. I. Takeuchi, O .O. Famodu, J. C. Read, M. A. Aronova, K. S. Chang, C. Craciunescu, S. E. Lofland, M. Wuttig, F. C. Wellstood, L. Knauss and A. Orozco, *Identification of novel compositions of ferromagnetic shape-memory alloys using compositional spreads*, Nature Mater. **2**, 180 (2003).
2. G. Kresse and J. Furthmüller, *Efficient iterative schemes for ab initio total energy calculations using a plane-wave set*, Phys. Rev. B **54**, 11169 (1996).
3. G. Kresse and D. Joubert, *From ultrasoft pseudopotentials to the projector augmented-wave method*, Phys. Rev. B **59**, 1758 (1999).
4. K. Parlinski, *PHONON* , (Cracow, Poland, 2002).
5. P. J. Webster, K. R. A. Ziebeck, S. L. Town and M. S.Peak, *Magnetic order and phase transformation in Ni_2MnGa*, Phil. Mag. **49**, 295 (1984).
6. C. Bungaro, K. M. Rabe and A. Dal Corso, *First-principles study of lattice instabilities in ferromagnetic Ni_2MnGa*, Phys. Rev. B **68**, 134104 (2003).
7. A. Dal Corso and S. de Gironcoli, *Ab initio phonon dispersion of Fe and Ni*, Phys. Rev. B **62**, 273 (2000).
8. A. T. Zayak, P. Entel, K. M. Rabe, W. A. Adeagbo and M. Acet, *Anomalous vibrational effects in non-magnetic and magnetic Heusler alloys*, Phys. Rev. B **72**, 054113 (2005).
9. A. Zheludev, S. M. Shapiro, P. Wochner and L. E. Tanner *Precursor effects and premartensitic transformation in Ni_2MnGa*, Phys. Rev. B **54**, 15045 (1996).
10. O. Delaire, M. Kresch and B. Fultz *Vibrational entropy of the γ-α martensitic transformation in $Fe_{71}Ni_{29}$* , Phil. Mag. **85**, 3567 (2005).
11. E. Maliszewski and S. Bednarski, *Lattice dynamics of $Fe_{0.65}Ni_{0.35}$ classical Invar*, phys. stat. sol. (b) **211**, 621 (1999).
12. E. Maliszewski and S. Bednarski, *The lattice dynamics of $Ni_{0.88}Fe_{0.12}$, $Ni_{0.76}Fe_{0.24}$ and Ni single crystals*, phys. stat. sol. (b) **200**, 435 (1997).
13. E. D. Hallman and B. N. Brockhouse, *Crystal dynamics of nickel-iron and copper-zinc alloys*, Can. J. Phys. **47**, 1117 (1969).
14. S. Baroni, S. de Gironcoli, A. Dal Corso and P. Giannozzi, *Plane-Wave Self-Consistent Field Method*, `http://www.pwscf.org`.